Tuning conjugated polymer chain packing for stretchable polymer semiconductor

*Jie Xu, Hung-Chin Wu, Jaewan Mun, Rui Ning, Weichen Wang, Shayla Nikzad, Hongping Yan, Xiaodan Gu, Shaochuan Luo, Dongshan Zhou, Jeffery B.-H. Tok, Zhenan Bao**

[*] Dr. J. Xu, Dr. H.-C. Wu, Dr. J. Mun, R. Ning, W. Wang, S. Nikzad, Dr. H. Yan, Dr. X. Gu, Dr. J. B.-H. Tok, Prof. Z. Bao
Department of Chemical Engineering, Stanford University, Stanford, CA 94305, USA
E-mail: zbao@stanford.edu

Dr. J. Xu
Nanoscience and Technology Division, Argonne National Laboratory, 9700 South Cass Avenue, Lemont, IL 60439, USA

Dr. H. Yan, Dr. X. Gu
Stanford Synchrotron Radiation Lightsource, SLAC National Accelerator Laboratory, Menlo Park, CA 94025, USA

Dr. S. Luo, Prof. D. Zhou
Department of Polymer Science and Engineering, School of Chemistry and Chemical Engineering, Nanjing University, Nanjing 210093, China

†Present address: Dr. X. Gu
School of Polymer Science and Engineering, University of Southern Mississippi, Hattiesburg, MS 39402, USA

Keywords: polymer semiconductor; molecular spacer; molecular ordering; charge transport; stretchable electronics

In order to apply polymer semiconductors to stretchable electronics, they need to be easily deformed under strain without being damaged. A small number of conjugated polymers, typically with semi-crystalline packing structures, have been reported to exhibit mechanical stretchability. Herein, we report a method to modify polymer semiconductor packing-structure using a molecular additive, dioctyl phthalate (DOP), as molecular spacers to insert between the amorphous chain networks and disrupt the crystalline packing. As a result, large-crystal growth is suppressed while short-range aggregations of conjugated polymers are promoted, which lead to an improved mechanical stretchability without affecting charge carrier transport. Due to the reduced conjugated polymer intermolecular interactions, strain-induced chain alignment and crystallization were observed. By adding DOP to conjugated polymers, we obtained stretchable

transistors with anisotropic charge carrier mobilities under strain, and stable current output under strain up to 100%.

1. Introduction

Stretchable conjugated polymers capable of performing electrical functionalities under mechanical deformation have applications ranging from skin-like electronics, soft robotics, to flexible energy harvesting and storage.[1-3] In conjugated polymers thin films, the charge carrier transport relies on the delocalization of charges through π-conjugation along backbones and π-π stacking across polymer chains. On the other hand, their mechanical stretchability depends on the dissipation of strain energy through changes in polymer chain conformations and chain packing microstructures.[4] Chemical structure designs, e.g., introducing soft non-conjugated segments[5,6] and dynamic bonds,[7] have improved mechanical deformability of conjugated polymers. However, the synthesizing new polymers may suffer in a decrease in charge mobility when a larger fraction of non-conjugated units are incorporated. Another strategy is blending conjugated polymers with elastomers.[8,9] When properly selected elastomers are used, they can result in nanoconfinement effect and improve the stretchability without sacrificing charge transport mobility. However, this approach requires specific device structures in order to achieve desirable vertical phase-separation morphologies. Even though it is well established that the polymer chain packing structures have a profound impact on the mechanical properties of conventional plastics,[10,11] the design principle of the suitable packing structures to simultaneously achieve good electrical charge transport and stable mechanical stretchability in conjugated polymers remains less understood.

The level of ease on polymer chain deformation under mechanical strain depends on its chain packing density. For example, loosely packed polymer chains possess weaker intermolecular interactions among the segments as compared to the densely packed ones, thus leading to a higher chain dynamic mobility.[12-14] In solid-state films, conjugated polymers

usually form semi-crystalline microstructures with pockets of dense packed structures (i.e., crystalline domains) connected by loosely packed disordered amorphous regions (**Figure 1a**).[15,16] Under a tensile strain, the amorphous phase may deform and the crystalline regions may undergo slips or distortions, both affected by the interplay between the amorphous network density and the size and stability of crystalline blocks.[17] To improve the stretchability of these conjugated polymer films, reducing the intercoupling among polymer segments in both amorphous and crystalline regions will allow easier regulations of polymer chain conformations and packing microstructures, hence dissipating strain energy more effectively during stretching.

Recent understanding on conjugated donor (D)-acceptor (A)-type polymers showed that high charge carrier mobilities can be achieved without large crystalline domains. The more important feature is the presence of "tie chains" connecting between aggregates.[8,15,18] This suggests that a polymer morphology with a large fraction of loosely-packed amorphous chains connecting small aggregates may have the potential to achieve both robust mechanical deformability and efficient charge transport though fine control of local structural packing.

To achieve a loosely-packed polymer film while having sufficient π - π stackings, we hypothesized that the following two key requirements need to be met during film formation: (i) increase the intersegmental proximity, and (ii) promote the formation of small aggregates while suppressing the growth of large crystal lamellae. However, conjugated polymers have a strong tendency to aggregate, leading to a fast crystallization kinetics during solvent evaporation process.[19] Therefore, normal film deposition (i.e., solution casting) from the solution will result in long-range ordered crystals and densely packed chains even within amorphous regions. Previously reported processing methods (e.g., annealing and seeding) have largely been applied to improve films' crystallinity or orderings, but are unfavorable to realize high mechanical stretchability. Recently, molecular solid additives were demonstrated to improve the strain tolerance of D-A conjugated polymers, but the charge carrier mobilities of these films were

negatively affected as seen by around one order of magnitude decrease in mobility at 100% strain.[20]

In this work, we examine the effect of a molecular additive, dioctyl phthalate (DOP), as bulky molecular fillers to increase free volume of the amorphous chain networks, weaken the interactions between crystalline laminar layers and suppress large-crystal growth. We observed that DOP promotes short-range aggregations of the D-A conjugated polymers used and maintains efficient charge carrier transport (**Figure 1a**). We further observed enhanced chain dynamics, polymer alignment and strain-induced crystallization under mechanical stimuli. This led to a substantial anisotropy in charge carrier mobilities. Subsequently fabricated stretchable transistors with DOP-treated conjugated polymers were observed to possess 5-time higher carrier mobility along the stretching direction than the perpendicular direction. In addition, it displayed a 2.5-fold charge carrier mobility enhancement compared to non-stretched film. Combined with device size design, the resulting transistors had stable current outputs when stretched up to 100% strain. One of the 'universal' logic gates, i.e., NOT gate, built using these transistors showed an almost geometry-independent logic operation and propagation delay, even when the device was stretched to twice of its original length.

2. Results and Discussion

2.1. Design of the packing structure modifiers

We describe here a design concept in selecting molecular fillers to modulate the polymer chain packing structures in order to achieve stretchable D-A conjugated polymers with high charge carrier mobilities. A common practice in the manufacturing of commodity polymers, high-boiling organic solvents are added as plasticizers for improved processability.[21] The plasticizers reduce intermolecular interactions through solubilizing polymer chains and reducing large crystal formation. Therefore, we hypothesize that inclusion of such molecules as "molecular fillers" may improve the stretchability of D-A conjugated polymers. These molecular fillers will potentially introduce conformational freedom for the polymer chains and

reduce crystallinity, while hopefully still provide short-range orders to allow efficient charge transport.

Three main considerations are listed for selection of suitable molecular fillers: (i) having a high-boiling point or a low volatility to allow tuning of the polymer microstructure development during the film formation process, (ii) desirable to reside with the side-chain groups instead of intercalating between conjugated backbones in order to maintain good charge transport (**Figure 1a**), (iii) having a relatively large molecular size to produce spaces among chain segments/crystalline intra-lamellae. To investigate the above described concept, we used poly[2,5-bis(4-decyltetradecyl)pyrrolo[3,4-c]pyrrole-1,4-(2H,5H)-dione-(E)-1,2-di(2,2′-bithiophen-5-yl)ethene] (DPPTVT), which is known as a high-mobility conjugated polymer with aromatic planar backbone and long branched alkyl side chains as the model polymer for this study (**Figure 1a**). To satisfy the above-described design criteria, we selected DOP as the additive molecular filler.[22,23] DOP contains bulky alkyl groups and has a high boiling point (385°C), which fits our hypothesized requirements.

2.2. Loosened chain packing structures

We performed in-depth characterizations of the DOP-modified DPPTVT polymer films to determine the impact of DOP on polymer packing structures. First, we investigated impact of DOP on DPPTVT solution aggregation states. Upon addition of 0.125 wt% of DOP to DPPTVT chlorobenzene solution, a substantially decreased solution viscosity was observed at low shear rates, as shown by the rheology measurements (**Figure 1b**). This indicates that the presence of DOP molecules results in a decrease of the interactions among DPPTVT polymer chains in the solution. From solution UV-vis spectroscopy characterization (Figure S1 in Supporting Information), DPPTVT exhibited slightly reduced relative absorption intensity at 805 nm (0-0 peak) upon addition of 0.125wt% of DOP in the solution state, which is attributed to the decrease in aggregation.[24]

The effect of DOP in modulating chain packing structures was next investigated on three type of films, namely: (i) neat films spin-coated from DPPTVT solution as reference samples, (ii) DOP films spin-coated from DPPTVT solution with 0.125 wt% of DOP, and (iii) DOP-r films prepared by extracting out the DOP from DOP film by methanol (Figure S2a (Supporting Information)). From both optical and atomic force microscopy (AFM) characterizations (Figures S2b and c), all three films exhibited smooth and homogenous morphology without observable phase separations, implying that the DOP molecules blended efficiently into DPPTVT polymer. The roughness of DOP-r film was slightly larger than that of the neat film, caused by removal of the DOP molecules from the polymer film. The glass transition temperature (T_g) of DPPTVT obtained by the differential AC chip calorimetric method showed a decreased value and an increased heat capacity (a bigger step of the differential voltage) for the DOP-r film compared to that of the neat film (**Figures 1c** and S3), which is an indication of enhanced polymer chain dynamics possibly due to the reduced packing density in the amorphous region of DOP-r film as empty spaces are created after DOP removal. Compared to the neat film, suppressed crystallization was observed in DOP and DOP-r films as seen from the decreased intensity of grazing incidence X-ray diffraction (GIXD) patterns (**Figure 1d**). In addition, after adding DOP, the laminar packing distance (*h00*) was observed to increase incrementally, from 24.5 A to 28.2 A, while the π - π stacking distance (*010*) remained unchanged (**Figures 1e** and S4). These characterizations indicate that the DOP molecules interrupted the crystallization of DPPTVT polymer during film formation and they reside mostly with the alkyl side-chains at the interlayer space of the laminar stacking in crystalline regions, which caused the increase of laminar spacing, and in the amorphous regions. The size of DOP molecule is obtained through DFT calculation at equilibrium state (Figure S5). Despite of the suppressing of long-range ordered crystals after adding DOP, the short-range ordered aggregations were still promoted in both the DOP and DOP-r films. This was indicated by an increased the ratio between the 0–0/0–1 peak and a slight redshift of the 0–0 peak from the

ultraviolet–visible spectrums (**Figure 1f**). These aggregates have been shown to be important for efficient charge transport in these films.[8,15] We will be further discussed the observation of charge transport towards the end of this paper (Figure S6). Both DOP and DOP-r films exhibited a decreased elastic modulus and a significantly increased stretchability (**Figures 1g-i**).

2.3. Alignment in strained films

Next, we investigate the mechanical adaptability of DOP treated DPPTVT films. The first examined feature was strain-induced alignment. We characterized the strained thin films using cross-polarized optical microscopy (CPOM), atomic force microscopy (AFM), followed by examining the 'orientational ordering' of polymer chains and crystalline regions using GIXD. For all studied films, CPOM showed light extinction under strain when the light polarization direction was parallel to the stretching direction, indicating polymer chain alignment along the strain direction. Uniform light re-emergence was observed once the stretched thin films were rotated 45^{o} with respect to the light polarization direction (**Figure 2a**). In addition, greater birefringence was detected as strain level increased, indicating a higher degree of polymer chain alignment was achieved. On the contrary, the 0% stain films did not exhibit observable polarization anisotropy. Note that the films prepared with DOP additives possessed much brighter CPOM images under strain as compared to neat DPPTVT films, indicating that greater freedom of polymer chain movement which is consistent with our hypothesis that DOP reduces DPPTVT intermolecular interaction. On the other hand, crack propagations were observed on neat film at 50% strain (**Figures 2a** and **b**), which will dissipate strain energy and reduce the chain alignment. The topographic information of three types of strained films characterized by AFM (**Figure 2b**) further supported our hypothesis that the DOP and DOP-r films are more deformable than the neat DPPTVT films. From AFM topographies, cracks of micron-scale were observed perpendicular to the stretching direction in neat films, while the DOP and DOP-r films exhibited continuous films without observable cracks. We further corroborated these results via

dichroic ratio measurement (i.e., the ratio between the absorption intensity parallel to the alignment direction and that perpendicular to the alignment direction) using UV-vis spectroscopy with polarized light (**Figure 2c** and S7). We observed that higher dichroic ratio values were measured for the films under larger strains. Those with DOP molecules would give higher dichroic ratios under the same strain, indicating that addition of DOP allows DPP-TVT polymers undergo greater chain movement and alignment. In addition, rotating GIXD measurements were applied to investigate the alignment of the crystalline regions (**Figure 2d**). A gradual increase in intensity of lamellar scattering peak *(200)* along the strained direction parallel to the incident beam was observed in the strained DOP-r film as compared to the perpendicular direction, indicating the presence of orientational order of the crystalline regions. Again, higher degrees of alignment of crystalline regions were observed with DOP treated strained films.

2.4. Strained-induced crystallization and change in crystalline packing

Next, GIXD was used to characterize strain-induced changes in crystalline regions (**Figure 3a).** A stretched polymer film was transferred onto a Si substrate and was exposed to the X-ray beam, which was set to be parallel with respect to the stretching direction with an incidence angle of 0.12°. Lamellar ordering (*h00*) and π-π stacking (*010*) signals were observed in the out-of-plane (q_z) and in-plane (q_{xy}) directions, respectively, indicative of a typical edge-on packing orientation for DPPTVT. The crystallographic parameters were extracted from (*200*) and (*010*) peaks in 2D diffraction patterns of neat, DOP-added, and DOP-r DPPTVT films under 0, 50, and 100% strain, as shown in **Figures 3b** and **c**, respectively. The intensities of the diffraction patterns were normalized by the thickness of polymer films. Similar to most reports on stretchable conjugated polymers,[7] the (*200*) signal of neat film was significantly weakened as the strain level was increased (**Figures 3b** and **c**) due to the breakage of crystalline domains by strain, as one of the means of dissipating strain energy. On the contrary, the intensity of the

(*200*) and (*010*) peak increased substantially in both stretched DOP and DOP-r films (**Figures 3b** and **c**). We further summed the GIXD intensities of (*200*) peaks from rotating x-ray measurements (**Figures 3d**, and S8) to calculate the overall changes of the crystallinity. Compared to 0% strain, the crystallinity decreased, as expected, for the neat DPPTVT film under 100% strain, while the crystallinity increased substantially for stretched DOP (by 40%) and DOP-r (by 50%) films. We attribute this observation to the easier chain re-arrangement under deformation, enabled by the more loosely packed structures. As discussed previously, the lamellar spacing of DPPTVT was enlarged by adding DOP molecules, this may also reduce the interlayer interactions in the crystalline region so that polymer chains could be more easily re-organized when the thin film was stretched. On the other hand, the π-π stacking distance remained the same under strain, while the laminar packing distanced decreased significantly up to 50% strain and was almost unchanged from 50-100% strain (**Figures 3e** and **f**). In contrast, the lamellar distance continued to increase from 0-100% strain for neat DPPTVT film. These results suggest that DOP molecules tend to reside between the lamellar layers of DPPTVT to cause an expanded structure, while this structure get compressed upon stretching, providing a mechanism for stain energy dissipation (Figure S9). When the strain is released, the lamellar packing distances of three relaxed films only partially changed back toward the original 0% strain films and stabilized in the following cycles (Figure S10).

2.5. Stretchable field-effect transistor arrays and logic circuit

With improved stretchability and stain-induced crystallization, stretchable transistor arrays fabricated using DOP-treated films exhibited anisotropic charge carrier mobilities under strain and resulted in stable current output under strain up to 100%. First, the influence of introducing DOP molecules in DPPTVT films on charge transport was investigated using field-effect transistors (FETs) (Figure S5). Semiconducting layers with various amounts of DOP (from 0 to 0.25 wt% of DPP-TVT solutions) were prepared on Si substrates with SiO_x as

dielectric layer. An averaged charge carrier mobility of approximately 1.4 $cm^2V^{-1}s^{-1}$ was obtained. Interestingly, the amount of DOP incorporated did not affect the resulting DPPTVT film charge transport, as evidenced from nearly identical transfer curves with or without DOP (Figure S5). Also, the charge carrier mobility did not change after removal of DOP using methanol washing. Although the incorporation of DOP reduced long-range crystalline order as seen earlier (**Figure 1d**), the short-range order was actually promoted (**Figure 1f**), maintaining a good charge transport.

Next, we investigated the electrical performance of DOP treated films in stretchable FET arrays (**Figure 4a**). The fabrication processes are shown in Figure S11 in Supporting Information. Typical transfer characteristics with negligible hysteresis was observed (**Figure 4b**), and an average mobility of ~0.6 $cm^2V^{-1}s^{-1}$ was achieved (**Figure 4c**). The stretchable transistor array was stretched from 0 to 100% in steady increments of 25%. Transfer curves and their corresponding mobility of the FETs with charge transport direction parallel or perpendicular to the strain direction are summarized in **Figures 4d, e,** and **f**, respectively. The mobility in the parallel direction, surprisingly, increased nearly linearly with strain. Mobility of >1.5 $cm^2V^{-1}s^{-1}$, a 2.5-fold enhancement compared to 0% strain film, was measured when the device was stretched at 100% strain. Such an enhancement in mobility is likely due to the strain-induced morphological alignment and ordering. Coupled with the increase in mobility, the on-current of transistors under strain in the parallel direction was observed to be stable combined with effects from changes in geometry of the source and drain electrodes (i.e., channel length and width) from stretching (**Figure 4e**). On the other hand, the mobility in perpendicular direction exhibited slight decrease because the polymer chains tend to align to the parallel direction by applied force, as evidenced via our obtained dichroic ratio measurement (**Figure 2c**). Also, larger charge transport anisotropy at higher strain levels was observed. However, stable on-state current was nevertheless recorded in perpendicular direction regardless of the applied strain (**Figure 4f**). Furthermore, these stretchable FET arrays exhibited stable and

robust device performances despite >1,000 repeated stretching cycles (**Figures 4g** and S12). As a comparison, both the strain effects on the mobilities and on-currents from the neat film were detrimentally affected (Figure S13). This stable on-current of DOP-treated films under strain is desirable for using them as semiconducting layer in a Pseudo-CMOS inverter with strain-insensitive propagation delay. As a proof of concept, we proceed to fabricate intrinsically stretchable Pseudo-E inverters using both DOP-r and neat film (**Figures 4g, h** and S14). Upon completion, the dynamic responses and the propagation delay time of the inverters under strain were subsequently investigated. Due to the stable on-currents upon stretching, the inverter using DOP-r film as the active layer showed a strain-insensitive delay at both rising and falling edges as compared to the circuit fabricated using the neat film. This proof-of-concept strain-suppression behavior is useful for simplifying the design of functional circuits without having to use more complex dynamic differential circuits[26] or incorporating strain engineering designs.[27]

3. Conclusion

We report a method to allow less dense packed conjugated polymer chain packing to facilitate mechanical deformation more easily under stains. We showed that a bulky high boiling point DOP molecule acted as a molecular spacer to increase amorphous fraction of chain networks and disrupt crystalline laminar layers, thus suppressing large-crystal growth and promoting short-range aggregations. Consequently, we attained an improved mechanical stretchability, while maintaining good charge carrier transport. Strain-induced crystallization was observed in the deformed DOP treated DPP-TVT film leading to an anisotropic charge carrier mobility. This also provided a ‘counterbalance’ to the geometric changes of the stretched device to give stable device output currents. Such mechanical improvement was seen with other conjugated polymers using other molecular spacers (Figures S15 and S16), suggesting our described

method for tuning conjugated polymer chain packing structures provides a route to stretchable semiconductors for skin-like electronics.

Supporting Information
Supporting Information is available from the Wiley Online Library or from the author.

Acknowledgements
J.X. and H.-C.W. contributed equally to this work. This work is supported by US Department of Energy, Office Basic Energy Sciences, Division of Material Science and Engineering, Program on Physical Behaviors of Materials (DE-SC0016523). J.X. acknowledges the Center for Nanoscale Materials, supported by the U.S. Department of Energy, Office of Science, under Contract No. DE-AC02-06CH11357. X.G. thanks National Science Foundation for partial support under award number DMR- 2047689. This work was partially performed at the Stanford Nano Shared Facilities (SNSF), supported by the National Science Foundation under award ECCS-1542152. GIXD experiments were carried out at the Stanford Synchrotron Radiation Laboratory (SSRL), a national user facility operated by Stanford University on behalf of the U.S. Department of Energy, Office of Basic Energy Sciences.

Received: ((will be filled in by the editorial staff))
Revised: ((will be filled in by the editorial staff))
Published online: ((will be filled in by the editorial staff))

References

[1] S. Wang, J. Xu, W. Wang, G.-J. N. Wang, R. Rastak, F. Molina-Lopez, J. W. Chung, S. Niu, V. R Feig, J. Lopez, T. Lei, S.-K. Kwon, Y. Kim, A. M Foudeh, A. Ehrlich, A. Gasperini, Y. Yun, B. Murmann, J. B-H Tok, Z. Bao, *Nature* **2018**, *555*, 83.

[2] E. W. H. Jager, E. Smela, O. Inganäs, *Science* **2000**, *290*, 1540.

[3] Z. Zhang, M. Liao, H. Lou, Y. Hu, X. Sun, H. Peng, *Adv. Mater.* **2018**, *30*, 1704261.

[4] S. E. Root, S. Savagatrup, A. D. Printz, D. Rodriquez, D. J. Lipomi, *Chem. Rev.* **2017**, *117*, 6467.

[5] H.-F. Wen, H.-C. Wu, J. Aimi, C.-C. Hung, Y.-C. Chiang, C.-C. Kuo, W.-C. Chen, *Macromolecules* **2017**, *50*, 4982.

[6] F. Sugiyama, A. T. Kleinschmidt, L. V. Kayser, M. A. Alkhadra, J. M.-H. Wan, A. S.-C. Chiang, D. Rodriquez, S. E. Root, S. Savagatrup, D. J. Lipomi, *Macromolecules* **2018**, *51*, 5944.

[7] J. Y. Oh, S. Rondeau-Gagné, Y.-C. Chiu, A. Chortos, F. Lissel, G.-J. N. Wang, B. C. Schroeder, T. Kurosawa, J. Lopez, T. Katsumata, J. Xu, C. Zhu, X. Gu, W.-G. Bae, Y. Kim, L. Jin, J. W. Chung, J. B.-H. Tok, Z. Bao, *Nature* **2016**, *539*, 411.

[8] J. Xu, S. Wang, G.-J. N. Wang, C. Zhu, S. Luo, L. Jin, X. Gu, S. Chen, V. R. Feig, J. W. F. To, S. Rondeau-Gagné, J. Park, B. C. Schroeder, C. Lu, J. Y. Oh, Y. Wang, Y. Kim, H. Yan, R. Sinclair, D. Zhou, G. Xue, B. Murmann, C. Linder, W. Cai, J. B.-H. Tok, J. W. Chung, Z. Bao, *Science* **2017**, *355*, 59.

[9] G. Zhang, M. McBride, N. Persson, S. Lee, T. J. Dunn, M. F. Toney, Z. Yuan, Y. H. Kwon, P. H. Chu, B. Risteen, E. Reichmanis, *Chem. Mater.* **2017**, *29*, 7645.

[10] K. S. Simis, A. Bistolfi, A. Bellare, L. A Pruitt, *Biomaterials* **2006**, *27*, 1688.

[11] I. M. Ward, J. Sweeney, *Mechanical properties of solid polymers*. **2012**, John Wiley & Sons.

[12] J. Xu, D. Li, J. Chen, L. Din, X. Wang, F. Tao, G. Xue, *Macromolecules* **2011**, *44*, 7445.

[13] J. Mark, K. Ngai, W. Graessley, L. Mandelkern, E. Samulski, J. Koenig, G. Wignall, *Physical Properties of Polymers*. **2004**, Cambridge University Press.

[14] E. Manias, V. Kuppa, *European Phys. J. E* **2002**, *8*, 193.

[15] R. Noriega, J. Rivnay, K. Vandewal, F. P. V. Koch, N. Stingelin, P. Smith, M. F. Toney, A. Salleo, *Nat. Mater.* **2013**, *12*, 1038.

[16] S. Luo, T. Wang, M. U. Ocheje, S. Zhang, J. Xu, Z. Qian, X. Gu, G. Xue, S. Rondeau-Gagné, J. Jiang, W. Hu, E. Zhuravlev, D. Zhou, *Macromolecules* **2020**, *53*, 4480.

[17] Y. Men, J. Rieger, G. Strobl, *Phys. Rev. Lett.* **2003**, *91*, 095502.

[18] D. Venkateshvaran, M. Nikolka, A. Sadhanala, V. Lemaur, M. Zelazny, M. Kepa, M. Hurhangee, A. J. Kronemeijer, V. Pecunia, I. Nasrallah, I. Romanov, K. Broch, I. McCulloch, D. Emin, Y. Olivier, J. Cornil, D. Beljonne, H. Sirringhaus, *Nature* **2014**, *515*, 384.

[19] S. Luo, N. Li, S. Zhang, C. Zhang, T. Qu, M. U. Ocheje, G. Xue, X. Gu, S. Rondeau-Gagné, W. Hu, S. Wang, C. Teng, D. Zhou, J. Xu, *Chem. Mater.* **2021**, *33*, 1637.

[20] J. Mun, J. Kang, Y. Zheng, S. Luo, Y. Wu, H. Gong, J.-C. Lai, H.-C. Wu, G. Xue, J. B.-H. Tok, Z. Bao, *Adv. Electronic Mater.* **2020**, *6*, 2000251.

[21] P. Walters, D. F. Cadogan, C. J. Howick, *Ullmann's Encyclopedia of Industrial Chemistry*, **2011**, Wiley-VCH.

[22] D. Zhou, L. Li, Y. Li, J. Zhang, G. Xue, *Macromolecules* **2003**, *36*, 4609.

[23] W. Jiang, C. Zuo, J. Hu, Q. Gu, W. Chen, G. Xue, *Macromolecules* **2008**, *41*, 5356.

[24] M. U. Ocheje, B. P. Charron, Y.-H. Cheng, C.-H. Chuang, A. Soldera, Y.-C. Chiu, S. Rondeau-Gagné, *Macromolecules* **2018**, *51*, 1336.

[25] G.-J. N. Wang, L. Shaw, J. Xu, T. Kurosawa, B. C. Schroeder, J. Y. Oh, S. J. Benight, Z. Bao, *Adv. Funct. Mater.* **2016**, *26*, 7254.

[26] C. Zhu, A. Chortos, Y. Wang, R. Pfattner, T. Lei, A. C. Hinckley, I. Pochorovski, X. Yan, J. W.-F. To, J. Y. Oh, J. B.-H. Tok, Z. Bao, B. Murmann, *Nat. Electronics* **2018**, *1*, 183.

[27] W. Wang, S. Wang, R. Rastak, Y. Ochiai, S. Niu, Y. Jiang, P. K. Arunachala, Y. Zheng, J. Xu, N. Matsuhisa, X. Yan, S.-K. Kwon, M. Miyakawa, Z. Zhang, R. Ning, A. M. Foudeh, Y. Yun, C. Linder, J. B.-H. Tok, Z. Bao, *Nat. Electronics* **2021**, *4*, 143.

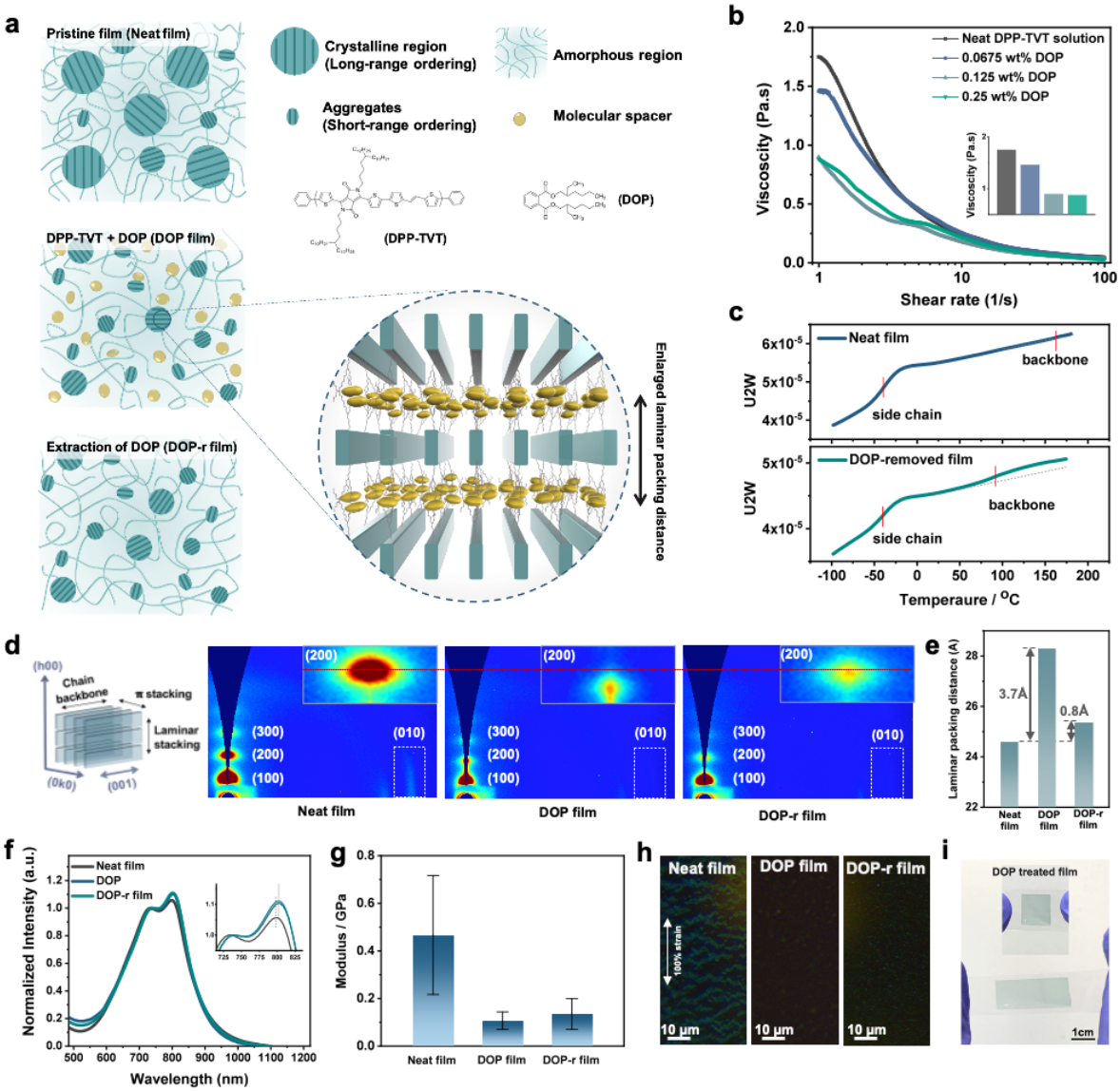

Figure 1. Loosened chain packing structures for improving the stretchability of conjugated polymers through solvent spacers. (a) Schematics of the chain packing morphologies before and after DOP treatment. (b) Rheological behavior of conjugated polymer solutions including different weight percentages of DOP. The insert shows the apparent viscosity of polymers solutions at shear rate of 1 s^{-1}. (c) Second heating curves from calorimetric ac-chip measurement for conjugated polymer films. (d) Schematic (left) of the packing structures in polymer films and GIXD images (middle) of the three films. In GIXD images, the dashed boxes highlight the in-plane π–π stacking peaks and the out-of-plane *(200)* laminar stacking peaks are zoomed out. (e) The laminar packing distance of three films calculated from *(200)* peaks. (f) Absorption spectra of ultraviolet–visible spectroscopy from three films. The insert shows the zoom-in spectra and the dash line is for guiding the eye. (g) Elastic moduli of the three films. (h) Dark field optical microscope images of the three films. (i) Photographs of a DOP-r film (blue) at 0% strain and stretched to 100% strain on a PDMS substrate.

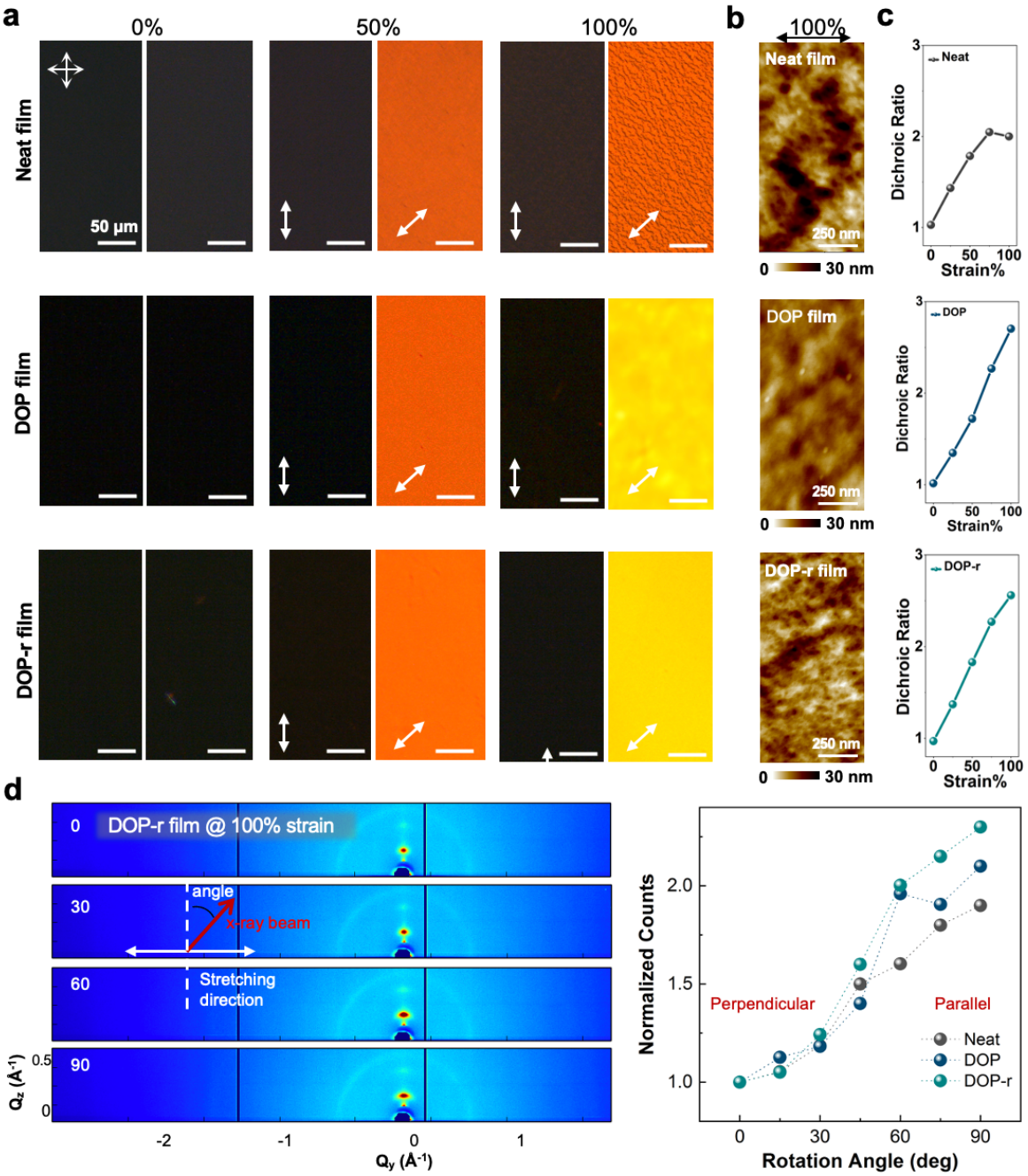

Figure 2. Morphological alignment resulted by stain-induced structure regulations. (a) Cross-polarized optical microscopic images. The orientation of the cross-polarizers is shown as crossed arrows, and the white arrows indicate the stretching direction. All scale bars are the same. (b) Tapping-mode AFM height images. (c) Dichroic ratios extracted from polarized UV-vis spectrums plot as a function of stretching strains. (d) GIXD images (left) of the DOP-r films under 100% strain, with the incident beam oriented at different angles to the stretching direction (90° is when the incident beam orientated parallel to the stretching direction). The right-hand

plot is the normalized intensity counts of *(200)* peak for the three films, with the incident beam oriented at different angles with respect to the stretching direction.

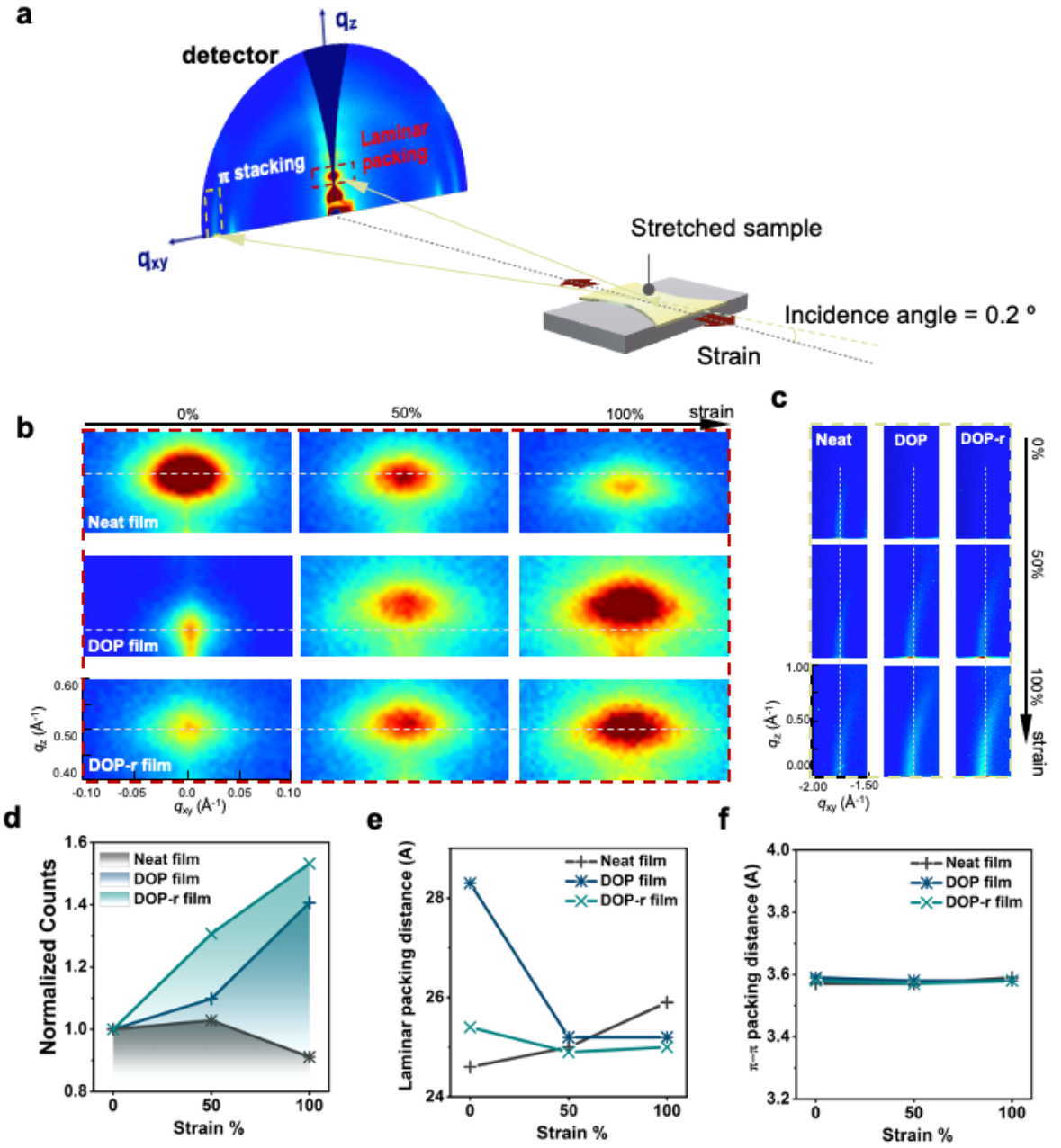

Figure 3. Changes of the crystal structure and the degree of crystallinity during stretching process. (a) Schematic of GIXD characterization of stretched films transferred on a Si substrate. (b,c) Comparison of *(200)* laminar scattering signals and *(010)* π-π stacking signals from GIXD measurements. The axis of each image are the same as marked in the bottom left image. (d) Normalized sum intensity counts of *(200)* scattering signals of three films characterized with the incident beam oriented at different angles with respect to each stretching direction. Plots of the (e) laminar packing distances and (f) π-π stacking distances in three films under different stretching strains.

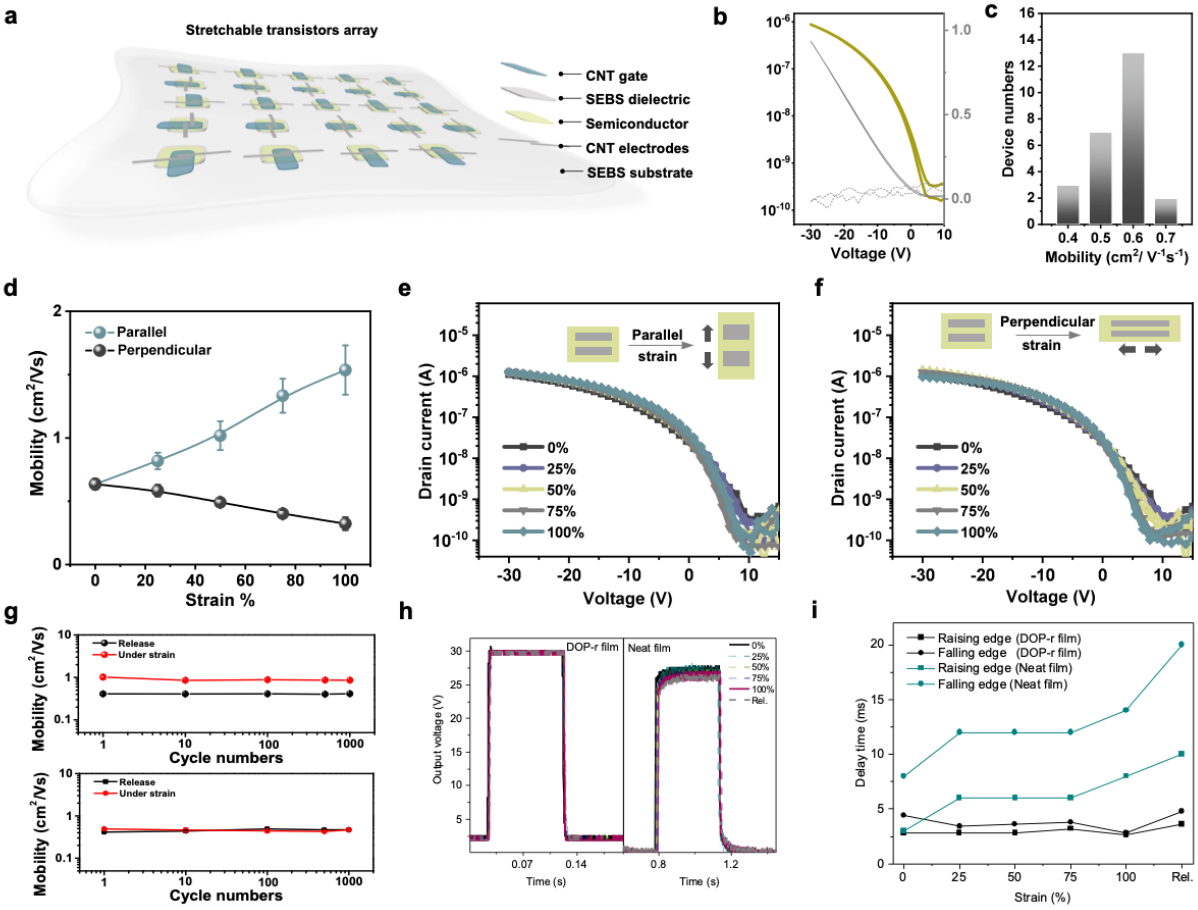

Figure 4. Fully stretchable transistor arrays and logic circuit fabricated from the DOP-r film. (a) Schematic of the device structure of a fully stretchable transistor arrays. (b) A typical transfer curve (V_D = −30 V) at 0% strain (gray line, square root of the drain current; dashed line, gate current). (c) Distribution of the mobility from 25 transistors in the arrays. (d) Changes in the mobility (calculated with measured device geometry and dielectric capacitance under strain) with strains up to 100%, both parallel to (blue) and perpendicular to (black) the charge transport direction. Changes in the transfer curves with strains up to 100%, both parallel to (e) and perpendicular to (f) the charge transport direction. (g) Changes in the mobility after multiple stretching-releasing cycles (up to 1000 cycles) at 50% strain, both parallel to (top) and perpendicular to (bottom) the charge transport direction. (h) Square wave signals of a fully stretchable inverters that fabricated by DOP-r film and neat film. (i) The propagation delay time of the inverters under strains.

Molecular spacers inserted between the amorphous chain networks can disrupt the crystalline ordering of polymer semiconductors. The long-range crystalline domains are suppressed while short-range aggregations of conjugated polymers are promoted, leading to an improved thin film stretchability without affecting charge transporting under an external strain up to 100%.

J. Xu, H.-C. Wu, J. Mun, R. Ning, W. Wang, S. Nikzad, H. Yan, X. Gu, S. Luo, D. Zhou, J. B-H Tok, Z. Bao*

Tuning conjugated polymer chain packing for stretchable polymer semiconductor

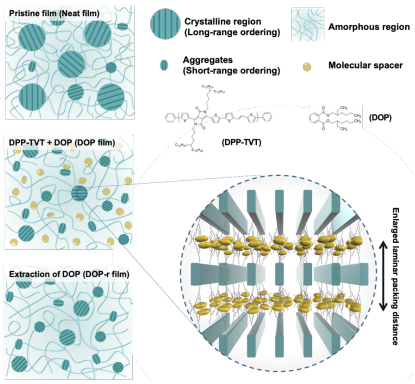

((Supporting Information can be included here using this template))

Supporting Information

Tuning conjugated polymer chain packing for stretchable polymer semiconductor

*Jie Xu, Hung-Chin Wu, Jaewon Mun, Rui Ning, Weichen Wang, Shayla Nikzad, Hongping Yan, Xiaodan Gu, Shaochuan Luo, Dongshan Zhou, Jeffery B-H Tok, Zhenan Bao**

Materials and Methods

Materials

DPPTVT was synthesized via reported method.[S1] The number-averaged molecular weight (Mn), weight-averaged molecular weight (Mw), and polydispersity index (PDI) of this polymer were 97.3 kDa, 387 kDa and 3.98, respectively, which were measured by high temperature size exclusion chromatography (SEC) and performed at 200 °C with 1,2,4-trichlorobenzene as the solvent on a Tosoh High-temperature EcoSEC equipped with a single TSK gel GPC column (GMHHR-H; 300 mm × 7.8 mm) calibrated with monodisperse polystyrene standards. SEBS (H1221 with volume fraction of poly(ethylene-co-butylene) = 88%, H1052 with volume fraction of poly(ethylene-co-butylene) = 80%,) was provided by Asahi Kasei. SEBS H1052 is used as dielectric layer and SEBS H1221 is used as elastomer substrate in fully stretchable devices. Poly (dimethylsiloxane) (PDMS, Sylgard 184, Dow Corning) was prepared at ratio of 12:1 (base/cross-linker, w/w) and cured at 70℃ overnight for use as the stretching substrate. and transferring stamp. DOP, octadecyltrichlorosilane (OTS) and all the solvents, such as chlorobenzene and trichloroethylene, were purchased from Sigma-Aldrich and used as received.

Thin films preparation and characterization

Solution preparation and characterization. Pristine DPPTVT solution was prepared by dissolving the conjugated polymers in chlorobenzene at a concentration of 2.5 mg/ml at 90 ℃ for 1 hr. DPPTVT solutions with DOP were prepared by mixing pre-dissolved conjugated

polymer solution (5 mg/ml in chlorobenzene) and different DOP solutions (1.25 mg/ml, 2.5 mg/ml and 5 mg/ml in chlorobenzene) at a volume ratio of 1:1 to yield the same DPPTVT concentration with the pristine DPPTVT solution. The amounts of DOP in solutions were calculated accordingly. The rheological behaviors of these solutions were characterized by a TA Instrument ARES-G2.

Substrate preparation. The bare Si or doped Si wafers with a SiO_2 dielectric (300 nm) were treated by a method published previously for forming a highly hydrophobic crystalline OTS monolayer on the surfaces.[S2] The wafers were cut into pieces (1.5 cm × 1.5 cm). Then a PDMS stamp (1.2 cm × 2.5 cm) was laminated on the middle area of the substrate to protect the OTS layer. Oxygen plasma (150 W, 200 mTorr of O_2 for 5 s) was used to remove the exposed OTS at the edges of the substrate in order to facilitate a more stable meniscus during coating. After removing the PDMS stamps and cleaning with toluene, the edge-etched OTS-modified substrates were ready for spin coating films. The modified bare Si were used as substrates for the GIXD characterization while modified Si/SiO_x were used as substrates for preparing devices.

Semiconducting films preparation. The neat DPPTVT film was spin-coated from the pristine DPPTVT solution at 1000 rpm for 1 min with a thickness around 20 nm. The DOP films were spin-coated from the DPPTVT solution with different amounts of DOP added at 1000 rpm for 1 min. The DOP-r film was prepared by extracting the DOP from DOP film in methanol (Figure S2) with a thickness around 20 nm. The thickness was characterized by profilometer (Bruker Dektak XT).

Morphology characterization. Optical images of the films were taken by a cross-polarized optical microscope (Leica DM4000M). The AFM images were performed with a tapping-mode AFM using a Multimode Nanoscope III (Digital Instruments/Veeco Metrology Group). UV-vis spectra were measured by an Agilent Cary 6000i UV/vis/NIR spectroscope, which was equipped with a rotational polarizer to measure the absorption intensity with the polarization parallel and perpendicular to the stretching directions. GIXD images in Figure 1d and Figure 3 were collected in a helium atmosphere at the Stanford Synchrotron Radiation Light source at beamline 11-3 and 7-2. The beam energy of beam 11-3 and 7-2 are 12.7 keV and 14 keV, respectively. The incidence angle of X-ray was 0.12º. Numerical integration of the diffraction peak areas was performed using WxDiff.

Electrical characterization. The initial electrical characterization was performed on bottom-gate, top-contact field effect transistors fabricated by directly spin-coating semiconducting

films on top of OTS-modified 300-nm-SiO_2/Si, then evaporating 40 nm Au. The channel length (L) and width (W) are 200 μm and 4 mm, respectively. The fabricated devices were stored under vacuum and tested using a probe station in an ambient environment connected to a Keithley 4200. The field-effect hole mobility μ was calculated in the saturation regime of transistor operation from the equation

$$\mu_{sat} = (\frac{\partial\sqrt{I_{DS}}}{\partial V_{GS}})^2(2L/WC_i),$$

where I_{DS} is the drain-source current, V_{GS} is the gate voltage, V_{DS} is the drain-source voltage and C_i is the capacitance per unit area.

Fully stretchable devices were prepared as a bottom-contact, top gate device structure according to our previously reported method.[S3] The channel length and width are 120 μm and 400 μm, respectively. The capacitance of dielectric layer was measured as 1.5 nF/cm^2. All the electrical characteristics of the devices were measured with a Keithley 4200 analyzer in an ambient environment. The mobility of semiconducting films was calculated with measured device geometry and dielectric capacitance under strain.[S3]

For the characterizations of the fully stretchable inverters, square wave signals generated from a function generator was used as the input signal. The output of the inverter was measured by an oscilloscope. Keithley 4200 was used as the DC power supply for the measurement. All these characterizations were performed in ambient.

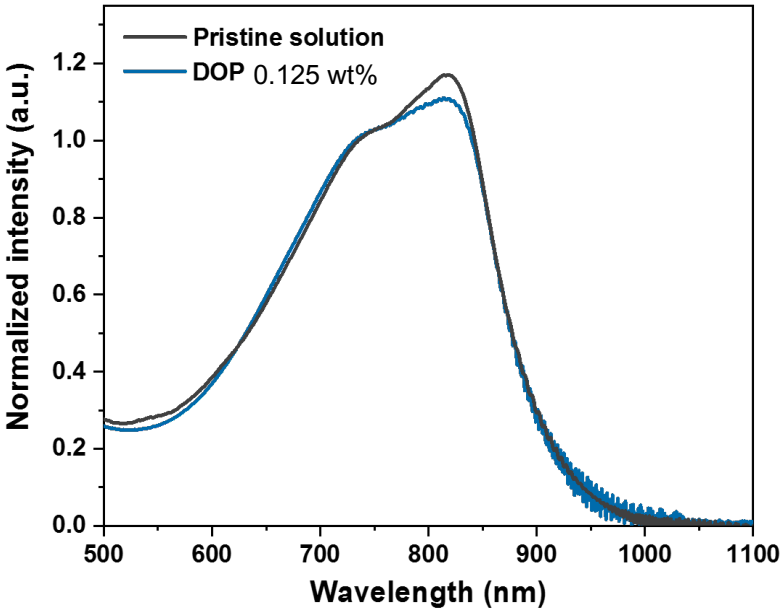

Figure S1. Normalized UV−vis absorption spectra of DPPTVT pristine solution and the solution with 0.125 wt% of DOP. Curves are normalized by the absorption peak centered at ca. 740 nm. Peaks at ca. 740 nm and 820 nm correspond to the (0-1) and (0-0) vibronic bands, which attributed to molecular coupling between donor and acceptor units. The aggregation behavior was determined by comparing the relative intensity of (0-1) and (0-0) peaks, which indicates a decrease in the aggregation for DPPTVT solution upon the addition of DOP.

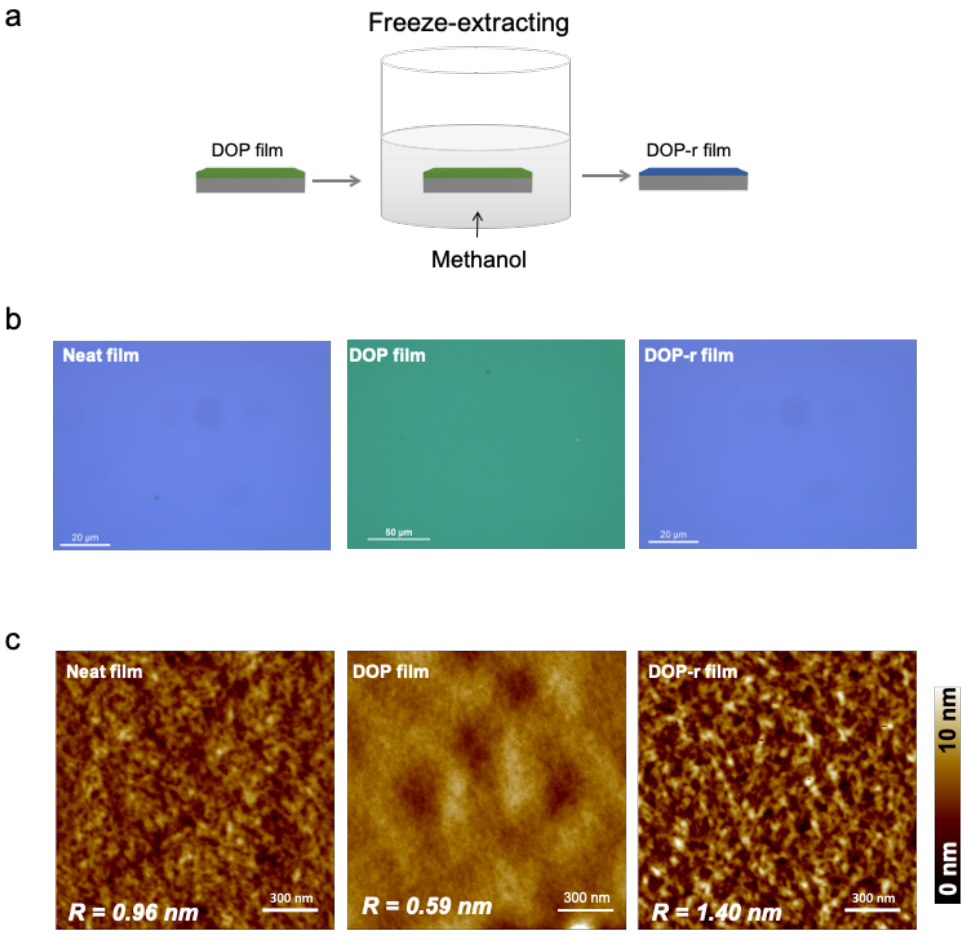

Figure S2. (a) Schematic diagram of experimental process in preparing DOP-r film. (b) Optical microscope images and (c) AFM height images of the neat, DOP, and DOP-r films.

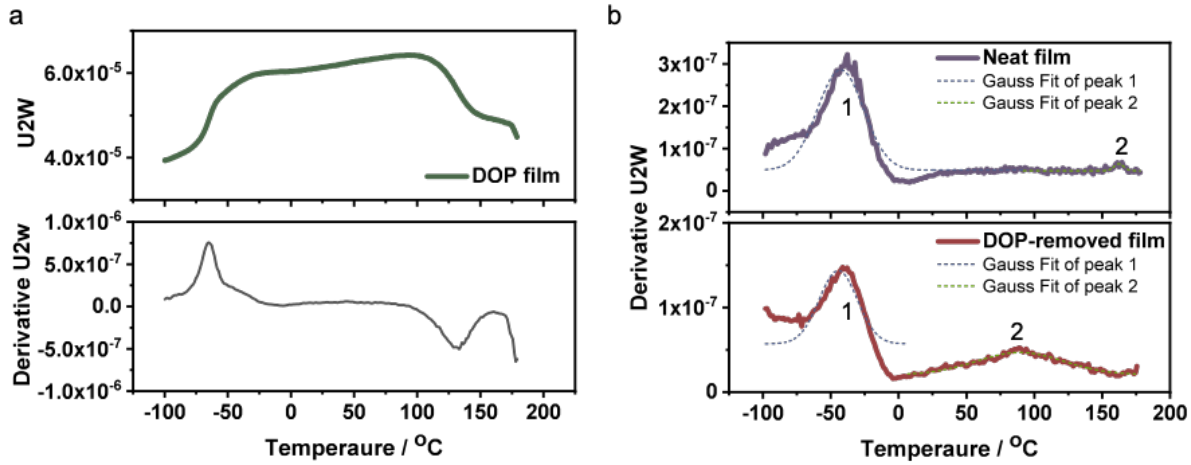

Figure S3. (a) AC chip calorimetry first heating scan (top) and its derivative (bottom) for the DOP film and (b) the neat DPPTVT film (top) and DOP-r film (bottom). As DOP molecules gradually evaporate from the thin film during the heating, the T_g of DPPTVT in DOP film cannot be determined. Fortunately, the polymer backbone T_g (peak 2 in (b)) can be observed after removing DOP molecules prior to heating process. The backbone T_g in the DOP-r film is significantly lower than in the neat film, demonstrating the effects of DOP incorporation on polymer chain dynamics.

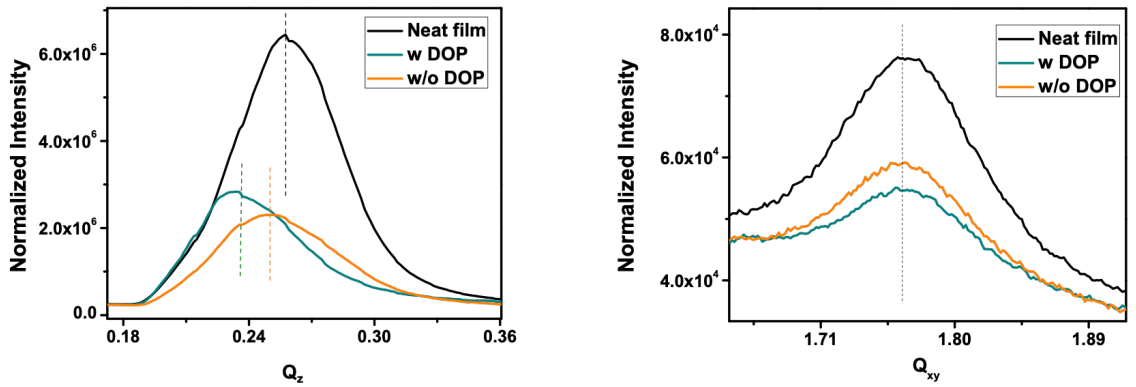

Figure S4. Line cut of lamella (in Q_z direction) and π-π stacking (in Q_{xy} direction) distance extracted from 2D GIXD patterns. Noticeable change of lamella spacing change was exhibited while the π-π stacking remained the same with and without DOP molecules in films. Note that the intensity of GIXD signals is normalized by the film thickness.

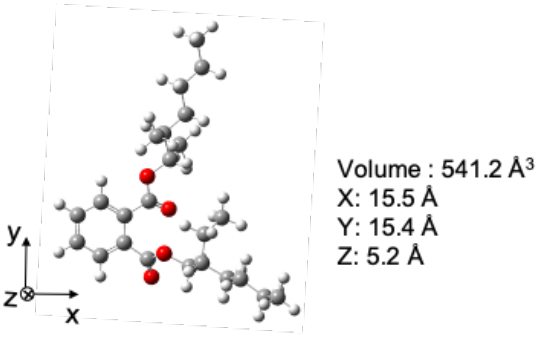

Figure S5. The size of DOP molecule obtained through DFT calculation at equilibrium state.

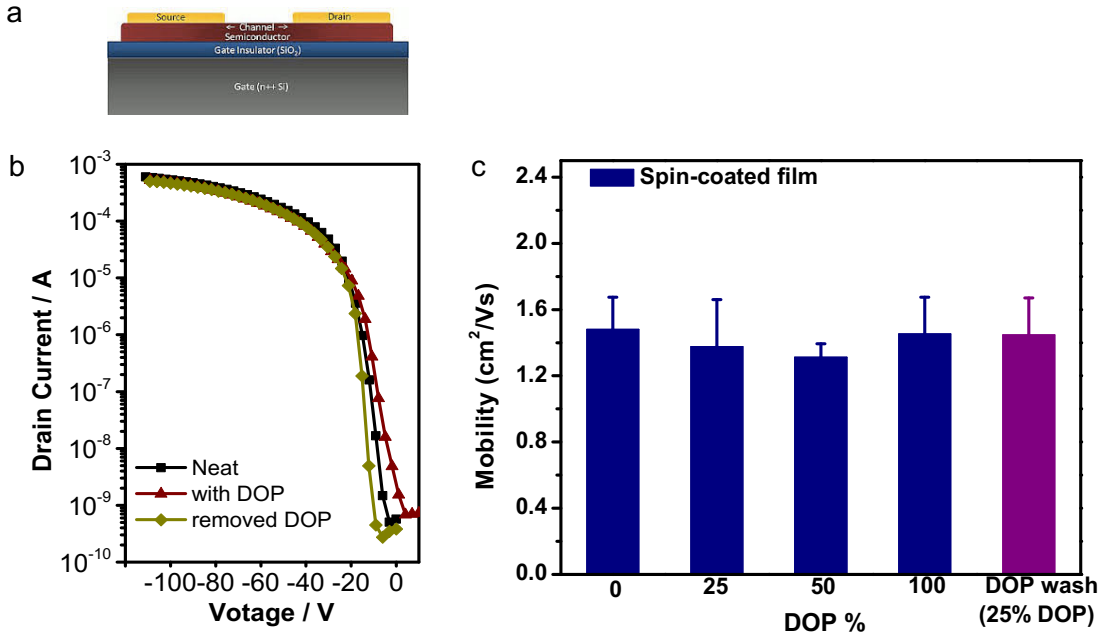

Figure S6. FET device characterizations. (a) Illustration of a bottom-gate/top-contact FET device. (b) Transfer curves of FET devices fabricated with neat, DOP, and DOP-r films. (c) Averaged charge carrier mobility of FETs based on thin films incorporated with various amount of DOP molecules (from 0 to 100%).

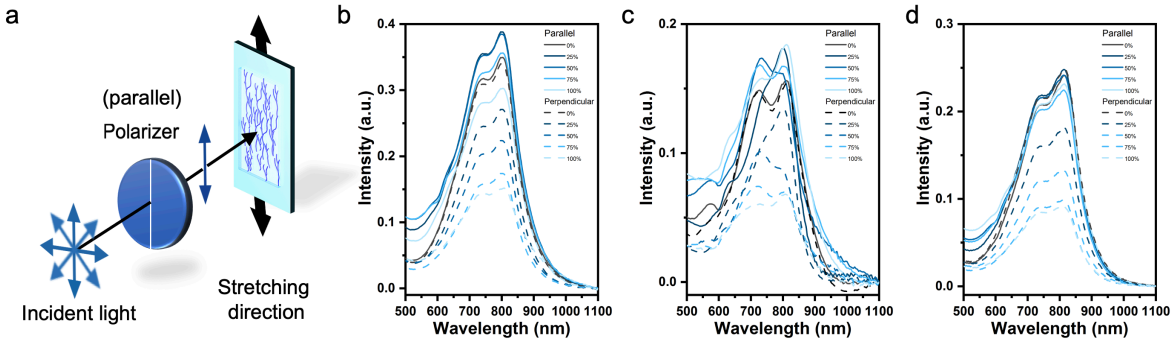

Figure S7. Absorption spectra of polarized UV-vis spectroscopy comparing neat, DOP, and DOP-r films under strains. (a) Schematic illustration of the characterization method. Parallel the film orientation when the stretching direction is parallel (perpendicular) to the axis of the polarizer. (b-d) The polarized UV spectra of (b) neat, (c) DOP and (d) DOP-r films.

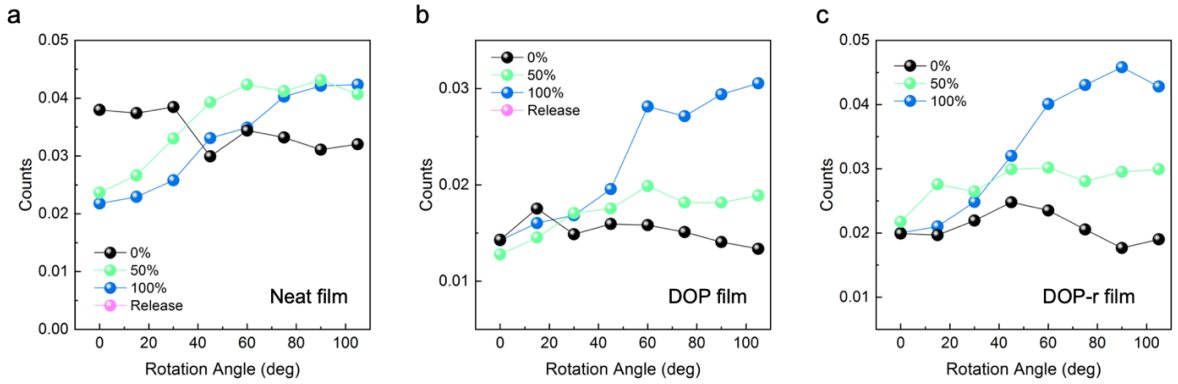

Figure S8. GIXD intensity of *(200)* diffraction signal versus sample rotation angle (i.e. 0° and 90° indicate the incident X-ray beam perpendicular and parallel to the stretching direction, respectively), for (a) neat, (b) DOP and (c) DOP-r films.

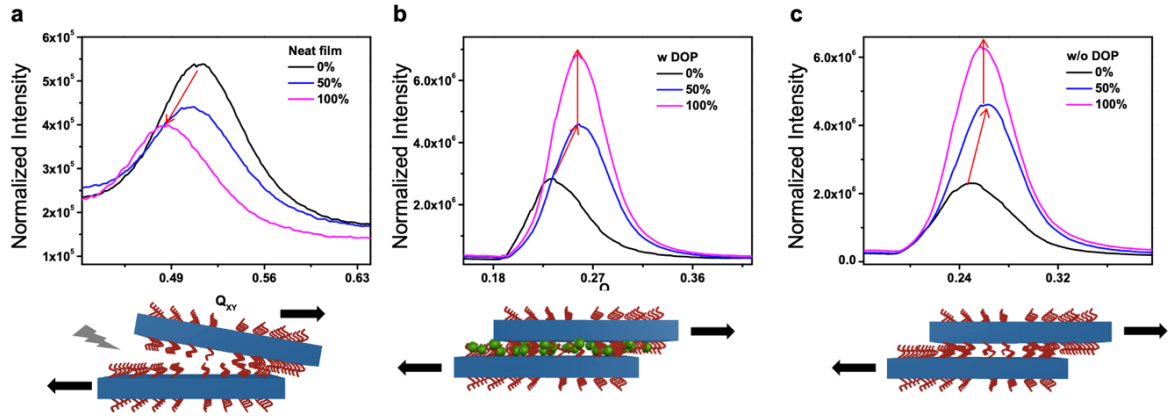

Figure S9. GIXD line cut of lamella (in Q_z direction) distance of the (a) neat, (b) DOP, and (c) DOP-r thin films under strain. The signals are normalized by the film thickness. The reduced intensity and enlarged spacing of neat film indicate the domain damage between polymer chains under strain, while DOP and DOP-r films exhibited reduced lamella spacing and strain-induced crystallization after deformation.

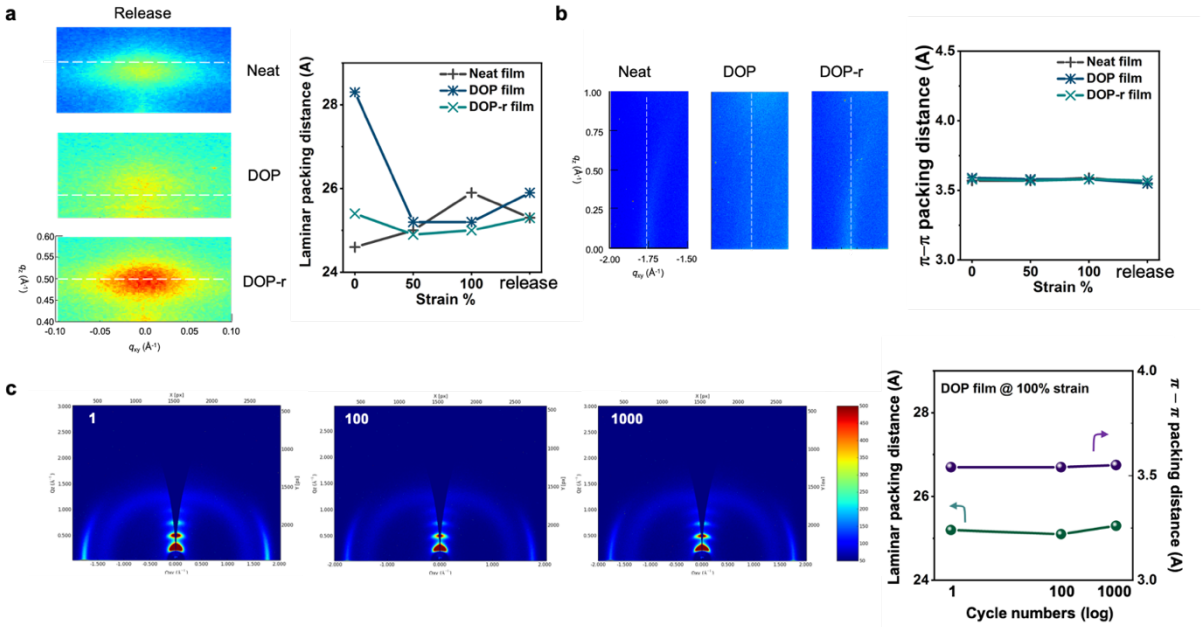

Figure S10. Changes of the crystal structure after release the strain and under 100% strains for different number of cycles. (a,b: left) When the strain (100%) is released, *(200)* laminar scattering signals and *(010)* π-π stacking signals from GIXD measurements in neat, DOP and. DOP-r films. Due to the wrinkles formation upon relaxation,[S4] the diffraction patterns of three relaxed films exhibit very weak intensities and cannot be used for the comparison of crystallinity. The white dash lines mark the center position of the scattering signals in pristine (0% strain) films. (a,b: right) Plots of the laminar packing distances and π-π stacking distances in three films before and after releasing the strain. (c) Two-dimensional GIXD pattern and plots of packing distances for DOP films under 100% strains for different number of cycles.

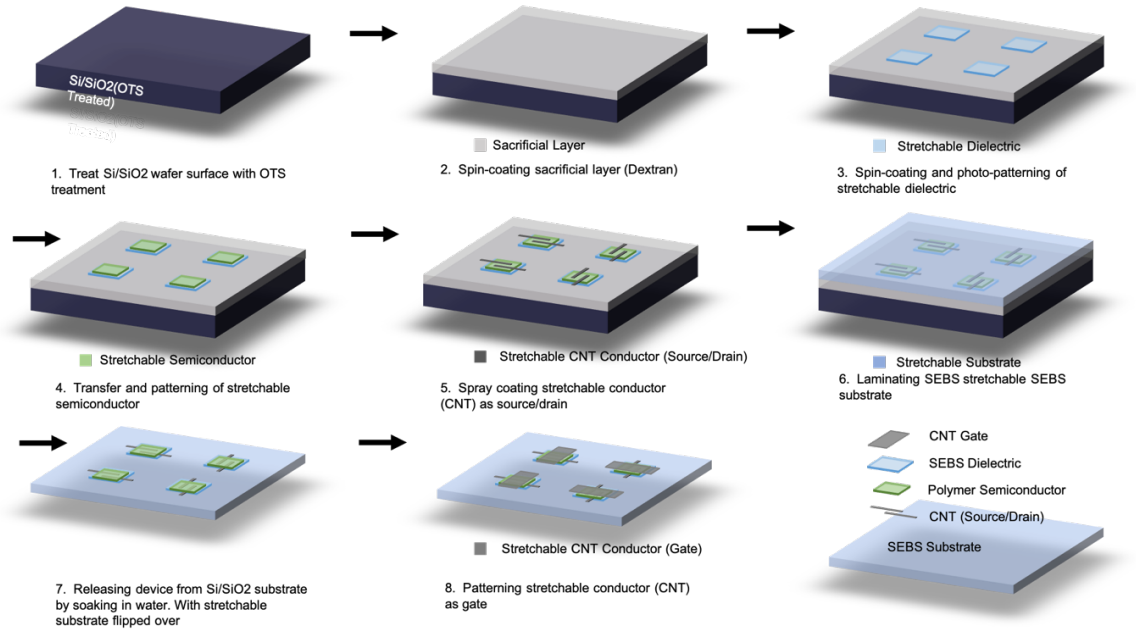

Figure S11. Schematic illustration of the manufacturing processes for making fully stretchable FET arrays.

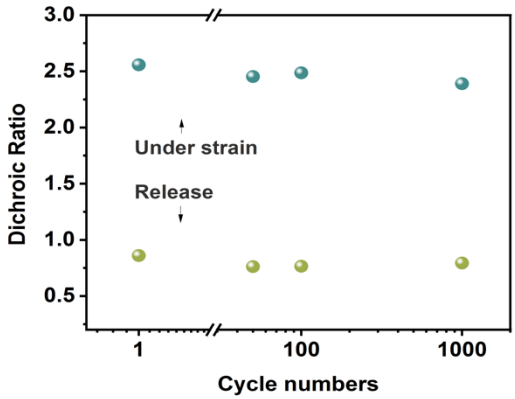

Figure S12. Dichroic ratios measurements for DOP-r films under 100% strains for different number of cycles. Stable and reproducible dichroic ratio values were exhibited under up to 1000 stretching/releasing cycles.

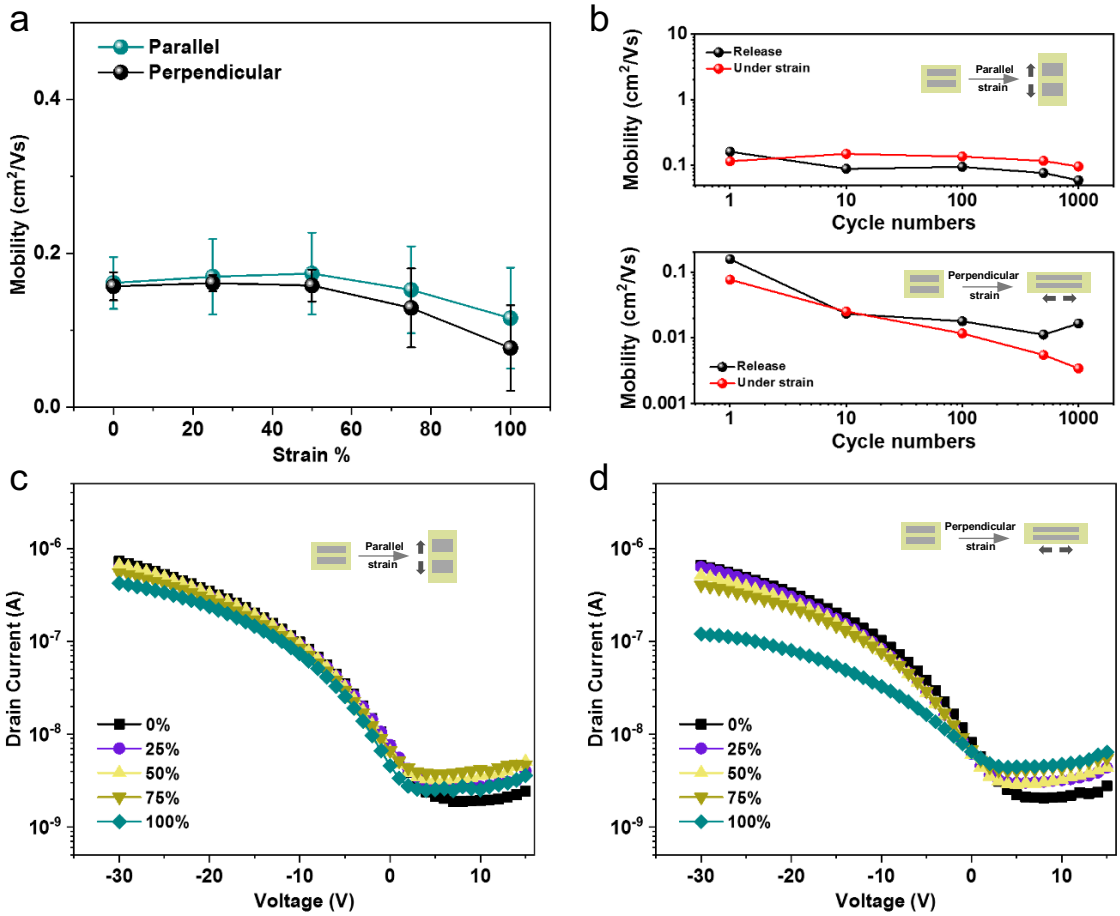

Figure S13. Electrical characteristics of fully stretchable FETs based on neat films. (a) Averaged charge carrier mobility as the charge transport direction parallel and perpendicular to the stretching direction. (b) Averaged mobility of the FETs under different numbers of stretch (at 50% strain)/release cycles. Both parallel (top) and perpendicular (bottom) directions were depicted. The corresponding transfer curves of the FETs in (c) parallel and (d) perpendicular directions under various strain levels. The source-to-drain voltage was set as -30V.

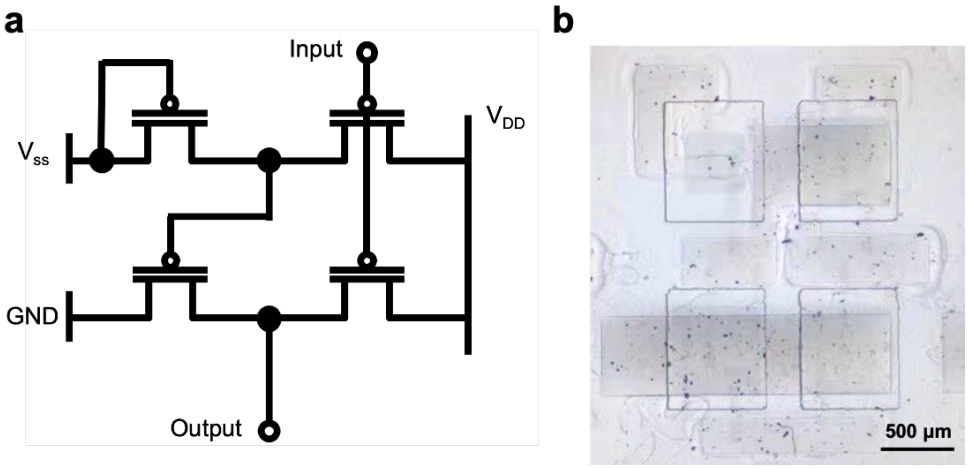

Figure S14. The (a) circuit diagram and (b) optical microscope image of a intrinsically stretchable Pseudo-E inverters.

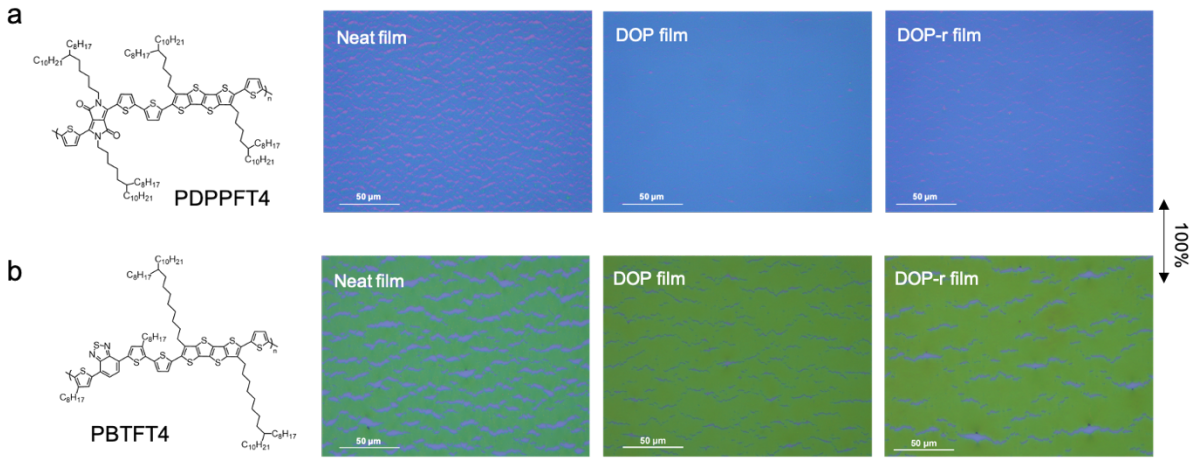

Figure S15. Optical microscope images of the stretched (at 100% strain) neat, DOP, and DOP-r films made of another two conjugated polymers. All the DOP and DOP-r films exhibit improved stretchability.

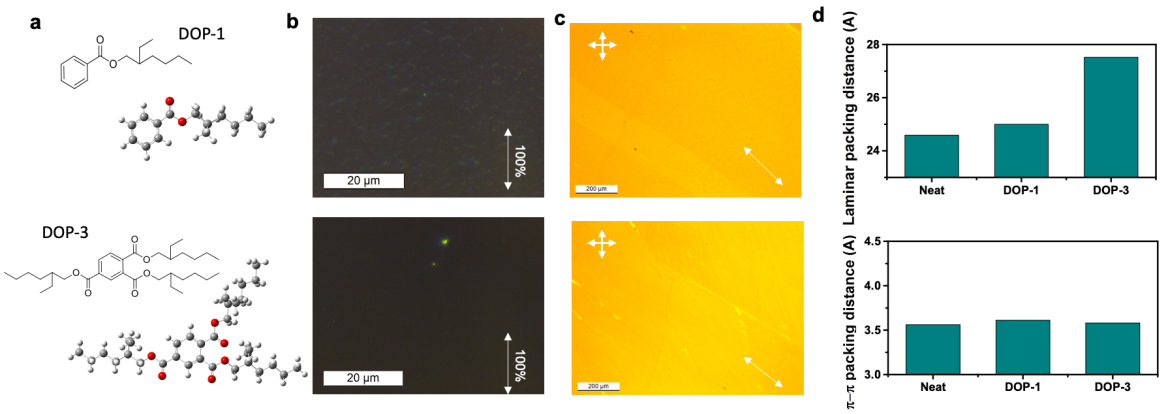

Figure S16. Two additional solvent additives are used for improving the mechanical stretchability of DPPTVT. (a) Chemical structures of two additives. (b) Dark field optical microscope images of the additives included films under 100% strain. (c) The laminar and π-π stacking packing distance of the additives included films.

Reference

[S1] G.-J. N. Wang, F. Molina-Lopez, H. Zhang, J. Xu, H.-C. Wu, J. Lopez, L. Shaw, J. Mun, Q. Zhang, S. Wang, A. Ehrlich, Z. Bao, *Macromolecules* **2018**, *51*, 4976.

[S2] A. Chortos, J. Lim, J. W. F. To, M. Vosgueritchian, T. J. Dusseault, T.-H. Kim, S. Hwang, Z. Bao, *Adv. Mater.* **2014**, *26*, 4253.

[S3] J. Xu, S. Wang, G.-J. N. Wang, C. Zhu, S. Luo, L. Jin, X. Gu, S. Chen, V. R. Feig, J. W. F. To, S. Rondeau-Gagné, J. Park, B. C. Schroeder, C. Lu, J. Y. Oh, Y. Wang, Y. Kim, H. Yan, R. Sinclair, D. Zhou, G. Xue, B. Murmann, C. Linder, W. Cai, J. B.-H. Tok, J. W. Chung, Z. Bao, *Science* **2017**, *355*, 59.

[S4] G.-J. N. Wang, L. Shaw, J. Xu, T. Kurosawa, B. C. Schroeder, J. Y. Oh, S. J. Benight, Z. Bao, *Adv. Funct. Mater.* **2016**, *26*, 7254.